Research Article | Vol. 10, No. 6 | 1 Jun 2019 | BIOMEDICAL OPTICS EXPRESS 2898
Biomedical Optics EXPRESS

Second harmonic generation microscopy of early embryonic mouse hearts

ANDREW L. LOPEZ III AND IRINA V. LARINA*

[1]*Department of Molecular Physiology and Biophysics, Baylor College of Medicine, One Baylor Plaza, Houston, TX 77030, USA*
**larina@bcm.edu*

Abstract: The understanding of biomechanical regulation of early heart development in genetic mouse models can contribute to improved management of congenital cardiovascular defects and embryonic cardiac failures in humans. The extracellular matrix (ECM), and particularly fibrillar collagen, are central to heart biomechanics, regulating tissue strength, elasticity and contractility. Here, we explore second harmonic generation (SHG) microscopy for visualization of establishing cardiac fibers such as collagen in mouse embryos through the earliest stages of development. We detected significant increase in SHG positive fibrillar content and organization over the first 24 hours after initiation of contractions. SHG microscopy revealed regions of higher fibrillar organization in regions of higher contractility and reduced fibrillar content and organization in mouse Mlc2a model with cardiac contractility defect, suggesting regulatory role of mechanical load in production and organization of structural fibers from the earliest stages. Simultaneous volumetric SHG and two-photon excitation microscopy of vital fluorescent reporter EGFP in the heart was demonstrated. In summary, these data set SHG microscopy as a valuable non-bias imaging tool to investigate mouse embryonic cardiogenesis and biomechanics.

1. Introduction

According to the American Heart Association, congenital heart defects (CHD) affect at least 8 per 1000 live births in the USA, and 1 in 150 adults have a form of CHD [1]. In order to improve our understanding of normal heart development, and enhance prevention and treatment of CHD, robust investigation of heart development in mammalian vertebrate models is essential.

All vertebrate hearts start with two bi-lateral heart fields derived from the mesoderm. They form myocardial vessels, that merge and twist on each other to make a linear heart tube. The linear heart expands, loops, and remodels to successfully establish aligned septate chambers in the mature heart [2]. During early embryogenesis, the heart also develops mechanically—from small foci of contracting cardiac progenitors, to a synchronous pump pushing blood through the circulation. How mechanical signals regulate cardiac development is a growing topic of interest. Experimental methods such as *ex vivo* embryo culture and microsurgeries have revealed that mechanical input is required for heart development, while loss of input can cause heart malformations and/or embryonic lethality [3–6]. Though informative, the relationship between mechanical input and heart development is not well understood because of technological limitations to study the mechanical microenvironment at the cellular level in a living beating heart.

The ECM plays a central role in determining the mechanical properties of the heart and is involved in mechanotransduction during heart development [7–11]. Often referred to as ‘cardiac jelly’, the ECM is a complex network of proteins that reside between the endocardium and myocardium to modulate cell phenotype and guide tissue development. Fibrillar collagen, a main constituent of the ECM, provides structural integrity, acts as a cell-signaling intermediary, and provides mechanical resistance for cardiomyocytes to contract.

#364419 https://doi.org/10.1364/BOE.10.002898
Journal © 2019 Received 9 Apr 2019; revised 15 May 2019; accepted 16 May 2019; published 21 May 2019

Biomedical Optics EXPRESS

Previous work in cell culture assays and biomaterial experiments have demonstrated that mechanical input regulates collagen production and fiber organization [4,12–17].

Visualization of fibrillar collagen in tissue through immunostaining can be challenging due to the variance between collagen subtypes, and its rod-like, rigid molecular structure which limits available epitopes for immunostaining. Additionally, the processing required for staining disrupts structural organization and makes identification of native structures challenging. However, due to their unique structure, collagen fibers can be visualized without labeling using second harmonic generation (SHG) microscopy. SHG microscopy is non-linear imaging approach that uses near-infrared light that interacts with non-centrosymmetric molecules, such as collagen. In a quantum effect, two photons of one frequency are combined to form one photon with double the frequency and half the wavelength. SHG microscopy is well established for investigation of fibrillar collagen networks in different tissues [18–20], though its application in early mouse embryonic hearts has not been explored.

In this work, we investigate SHG microscopy as a means to assess complexity and organization of structural fibers, including collagen, in the embryonic mouse heart. Collagen is known to be the strongest generator of SHG signal, but since the sarcomeres, actin and microtubules contribute to SHG signal as well [19,21], in this manuscript we refer to SHG positive fibers in the heart as fibrillar structures rather than collagen fibers. We present a protocol for SHG microscopy of embryonic mouse hearts from the earliest stages of contraction, and demonstrate developmental and regional differences in fibrillar content and organization that coincide with areas of differential mechanical load. We coupled SHG and two-photon fluorescence imaging of EGFP to expand the potential of future investigations on cellular processes in the context of heart mechanical homeostasis. These results demonstrate that SHG microscopy reveals valuable structural information in early cardiogenesis and can be a valuable tool to investigate embryonic cardiac biomechanics in mouse models.

2. Materials and methods

2.1 Mouse lines and embryo manipulation procedures

All procedures involving animals were performed according to protocols approved by the Institutional Animal Care and Use Committee at the Baylor College of Medicine. To acquire mouse embryos of desired developmental stages, timed matings were set overnight, and females were checked every morning for a presence of a vaginal plug. When a vaginal plug is confirmed, it is counted as embryonic day (E) 0.5. In this study, we used embryos at developmental stages E8.5-E9.5. At the desired developmental stage, embryos were dissected out of the uterus as described previously [22,23]. The dissection was performed in ice-cold phosphate buffered saline (PBS) (Sigma-Aldrich, Inc., St. Louis, MO, USA) pH7.4, and each embryo was collected in a glass vial filled with PBS kept on ice. Embryos were fixed in 4% paraformaldehyde/PBS (Electron Microscopy Sciences, Hatfield, PA, USA) at 4°C for one hour, washed three times in PBS for 10 min at 4°C, and stored in PBS at 4°C until imaging. Prior to imaging, embryos were positioned flat, ventral side up, and attached to a microscope slide or are mounted onto a 2% agarose bed and covered with a coverslip.

For experiments involving simultaneous imaging of SHG and two-photon fluorescence of EGFP, embryos were generated by crossing homozygous nTnG reporter mice [24] to homozygous Nkx2.5 IRES-Cre mice [25], which resulted in EGFP nuclear labeling on Nkx2.5 positive embryonic cardiac cells.

Mlc2a null embryos with deficient cardiac contractility were generated by crossing heterozygous Mlc2a mice [26]. Embryos were processed for SHG imaging as described above, and yolk sacs were separated for DNA isolation and PCR genotyping.

Biomedical Optics EXPRESS

2.2 Second harmonic generation, two-photon excitation, and brightfield microscopic imaging

SHG images were obtained with a Zeiss W Plan-Apochromat 20x/1NA water immersion objective on a Zeiss LSM7 multi-photon microscope with a tunable Chameleon Ultra II Ti:Sapphire laser (Coherent, Inc., CA, USA). SHG images were collected in the backwards direction. Validation of SHG imaging was performed using an FT445 dichroic mirror and a ZET405/20x filter (Chroma Technology Corp, VT, USA) with laser illumination set from 770 nm to 840 nm with 10 nm increments at 50% of power. Volumetric SHG imaging was performed using the FT445 dichroic mirror and the ZET405/20x or a BP380-430 filter with the laser set to 830 nm at 20-30% power. Simultaneous detection of SHG and two-photon excitation of EGFP fluorescence was performed using the FT490 dichroic mirror, the ZET405/20x filter for the SHG channel, and a BP500-550 filter for the EGFP channel. The laser was set to 830 nm at 20% of total power. Brightfield microscopic imaging was performed using a Zeiss Stemi 508 microscope at 5x magnification with a Zeiss Axiocam ERc5s camera.

All images were rendered in ZEN Blue (Carl Zeiss Inc., Thornwood, NY, USA) and Imaris software (Bitplane, Switzerland). Quantification of SHG positive fibrillar network in Mlc2a and control hearts was performed using open-source CT-FIRE V2.0 Beta software (https://loci.wisc.edu/software/ctfire) on maximum intensity projections of corresponding volumetric data sets.

3. Results and discussion

3.1 Validation of second harmonic generation imaging of fibrillar structures in the embryonic mouse heart

To confirm that the fibrillar structures observed in the images of the embryonic hearts were indeed produced by SHG, imaging was performed at different illumination wavelengths ranging from 770 nm to 840 nm at 10 nm increments using a narrowband emission filter 405/20 nm. Figure 1 presents the images of the same single plane within a ventricular heart wall of an E8.5 embryo. Since the wavelength of the SHG signal is one-half the illumination wavelength, using the 405/20 nm emission filter, the detection of the SHG signal is expected at illumination wavelengths of 790 to 830 nm. In Fig. 1, the fibrillar structures are most apparent in the range from 800nm to 830nm with lower levels of detection at the border wavelengths of 790 nm and 830 nm. Beyond this spectral region, the fibrillar components in the images disappear,

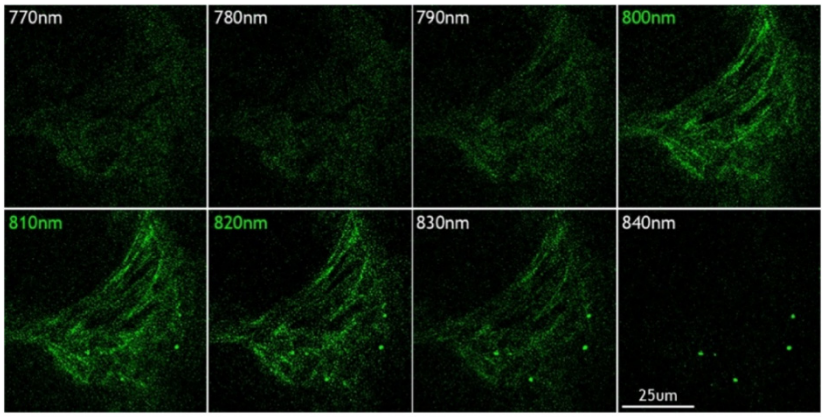

Fig. 1. Validation of SHG nature of cardiac fibrillar structures. Images of a single plane within an E8.5 heart ventricle wall at illumination wavelengths between 770 and 840 nm with 10 nm increment acquired through a narrowband emission filter 405 ± 10 nm. The illumination wavelength is labeled in the top left corner of each image. The detection and visualization were performed using the same settings for all images.

Biomedical Optics EXPRESS

demonstrating that the fibers in the images of the embryonic hearts are produced by SHG rather than two-photon excitation autofluorescence, and that the SHG signal is dominant over the two-photon excitation in this spectral range.

3.2 SHG positive fibrillar content and organization change as the heart develops

The mouse embryonic heart starts to contract at E8.5, and within 24 hours undergoes extensive changes in morphology and function. To more precisely stage heart development, the number of embryonic somites is recorded since a pair is added every 90 minutes. First contractions start at approximately 3 somite stage, while the heart is a linear tube. Within 4-5 hours after the first contractions, the heart lumen expands and cardiac function becomes stronger as it starts to circulate plasma through the vascular system of the embryo and the yolk sac. At the same time, the linear heart tube breaks symmetry and starts to balloon rightward toward a "jogging heart" stage (Figs. 2(A)-(C)). At 7-8 somite stage, first blood cells enter the circulation from the blood island. Figures 2(D)-(F) and Visualization 1 show corresponding changes in the content and organization of SHG positive fibrillar structures in the same embryonic hearts as in Panels A-C. SHG microscopy clearly shows a progressive increase in content and higher level of organization in fibrillar structures as the heart expands and undergoes cardiac looping. This demonstrates that SHG imaging reveals structural details heart fibers and can clearly differentiate changes in fibrillar organization within the developing heart at the earliest stages, which are not accessible with other approaches.

Third harmonic generation (THG) microscopy might provide complimentary information to SHG microscopy about molecular composition and structural components of developing embryonic hearts without staining. In contrast to SHG, THG microscopy picks up cellular and intracellular interfaces and optical heterogeneities in biological samples [27–29] as well as hemoglobin, which allows visualization of red blood cells [29,30]. The potential of THG microscopy toward investigation of embryonic cardiac development is a subject of future investigations.

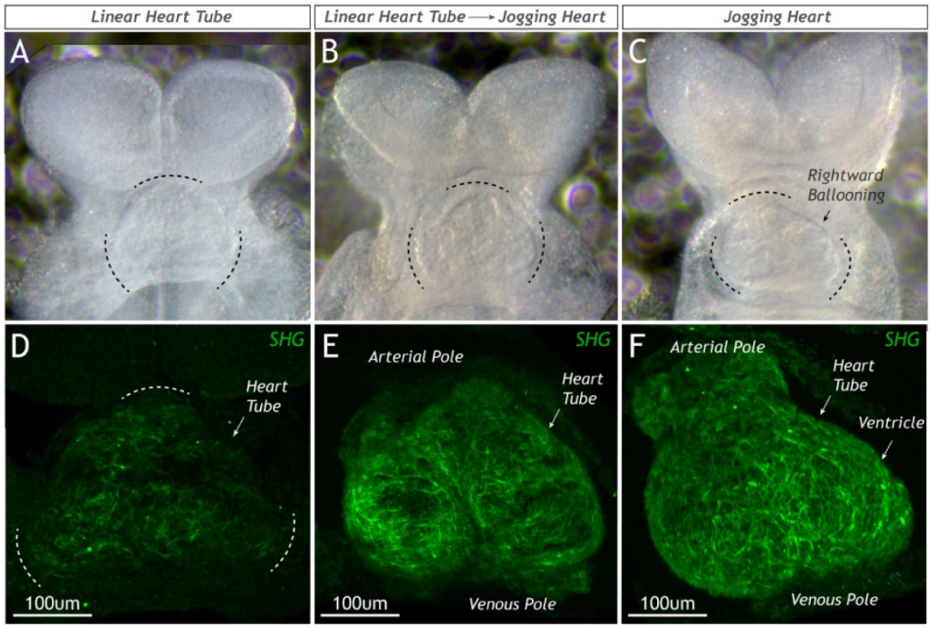

Fig. 2. SHG positive cardiac fibers develop quickly after beginning of heart contraction. (A-C) Brightfield images of mouse embryos focused on cardiac region at 3-4, 5-6, and 6-7 somite stages, respectively. (D-F) Corresponding 3-D SHG images of the same embryonic hearts as in (A-C). The image acquisition, rendering, and visualization were performed at the same settings. Visualization 1 shows volumetric details of SHG images in panels (D-F).

Biomedical Optics EXPRESS

3.3 Regional difference in SHG positive cardiac fibers

By 10 somite stage (about 10 hours after initiation of contraction), the heart beat becomes stronger, and blood circulation through the embryonic vasculature is well established. By this stage, the regional differences in SHG positive cardiac fibers becomes obvious (Fig. 3 and Visualization 2). Figure 3(A) shows a volumetric reconstruction of a 10 somite heart with a primitive ventricle and an outflow tract in view. The fibrillar organization is well resolved throughout the heart. Figures 3(B) and 3(C) show cross-sections through the 3-D data set at

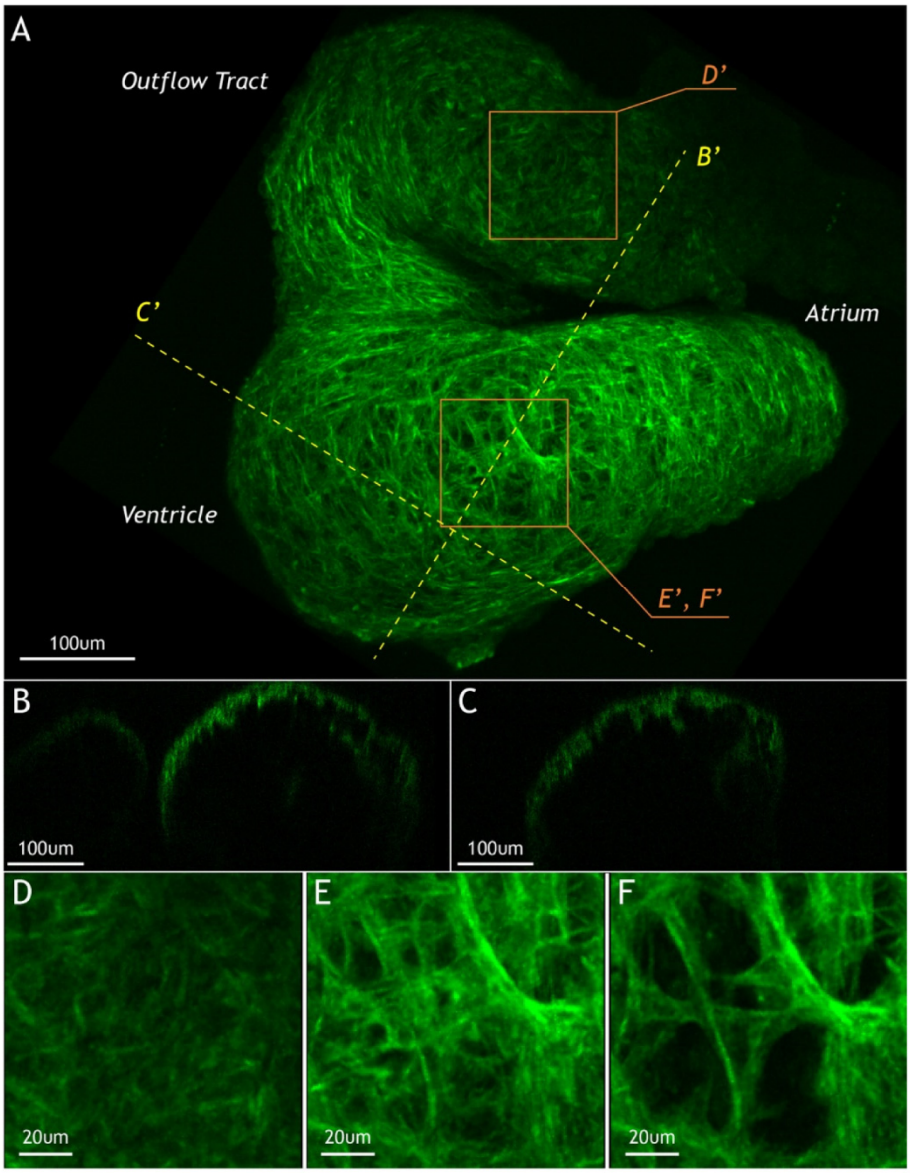

Fig. 3. SHG positive cardiac fibers show regional difference. (A) 3-D SHG imaging of the embryonic heart at E8.5 10-somite stage showing a ventricle and an outflow tract; the volumetric view is presented in Visualization 2. (B-C) Corresponding cross-sectional views through the heart at the planes labeled in (A). (D-F) Magnified view of the corresponding areas labeled in panel (A). (D) Magnified view of the outflow tract region labeled in panel (A). (E) Magnified view of the ventricle region labeled in panel (A). (F) The same region of the ventricle as shown in panel (E), but with a clipping plane at 15 um below the heart surface.

Biomedical Optics EXPRESS

positions labeled in A, demonstrating that the imaging depth is sufficient for visualization of fibrillar network through the depth of the heart wall. The magnified views of the labeled regions within the outflow tract and the ventricle are shown in Figs. 3(D) and 3(E), respectively. The ventricle, which is an actively contracting region, shows bright, well organized, and a clearly distinguishable network of fibers (Fig. 3(E)). Conversely, the outflow tract is a passively contracting region. The SHG signal in the outflow tract is weaker, the fibers are not clearly distinguishable, and not as organized as those in the primitive ventricle. This observation suggests that cardiac fibers and their level of organization coincide with regions of higher mechanical load, potentially providing an opportunity to study structure-function relationship in early cardiogenesis.

Interestingly, by this early stage, there is already heterogeneity of fibrillar organization in depth within the heart wall. For example, Fig. 3(F) shows the SHG signal within the same region of the ventricle as shown in Fig. 3(E), but with a clipping plane at 15 um from the heart surface. Cropping the top layer from the reconstruction and exposing the underneath layer reveals that a top fibrillar network layer is dense and interconnected, while the fibers in the underneath layer are longer, thicker and more spaced out. These thicker longer fibers in the underneath layer could be a basis for trabeculation development in the ventricle. Abnormal development of trabeculation is associated with congenital heart defects [5,31,32], and the presented approach could provide a useful tool to investigate the process of cardiac compaction and trabeculation in genetic mouse models.

Optical methods provide an advantageous opportunity to explore heart biomechanics because they are non-contact and can be used to manipulate mechanics within a physiological threshold. Currently, great advances are being made with optical methods such as cardiac laser-pacing and functional optical coherence tomography to analyze mechanics and function in the developing vertebrate heart [22,33–41]. Integration of the SHG microscopy with these analyses will provide means to assess how contractility regulates the content and organization of structural fibers including the ECM protein collagen—a determinant of tissue rigidity and elastic recoil.

3.4 SHG microscopy of genetic mouse model with cardiovascular defect

Well established genetic tools to manipulate the mouse genome that recapitulate models of human disease have provided thousands of genetic mouse models linked to cardiac development and cardiac failure, serving as a tremendous resource to study embryonic heart failure in mouse models at early stages, which cannot be resolved during human development. To investigate whether SHG microscopy can provide useful insight for investigation of genetic mouse models with cardiac defects, we performed SHG imaging of hearts in Myosin light chain 2a (Mlc2a) knockout (KO) embryos. Mlc2a KO embryos exhibit reduced cardiac contractility and are embryonic lethal by approximately E11.0. We focused our analysis at E9.5, about 24 hours after initiation of contraction (Fig. 4 and Visualization 3). Brightfield microscopic images of dissected hearts from the control and Mlc2a KO embryos are shown in Figs. 4(A) and 4(E), respectively. The whole control and Mlc2a KO embryos are shown in Figs. 4(B) and 4(F), respectively. By this stage, the morphological difference between the mutant and the control hearts becomes noticeable with the mutant heart showing signs of edema and improper looping. The corresponding 3D SHG microscopy images (Figs. 4(C) and 4(G) and Visualization 3) show a more developed fibrillar network in the atrium of the control heart with brighter, longer and more interconnected fibers. The SHG positive fibers in the Mlc2a KO heart are dimmer, shorter and less interconnected than in the control. Quantification of SHG positive fibrillar network shows the presence of longer and overall higher number of fibers in the control relative to the Mlc2a mutant (Figs. 4(D) and 4(H)). These results support the biomechanical role of heart contraction in cardiac morphogenesis and demonstrate a potential for SHG imaging in structural assessment of mouse genetic models with cardiac defects.

Biomedical Optics EXPRESS

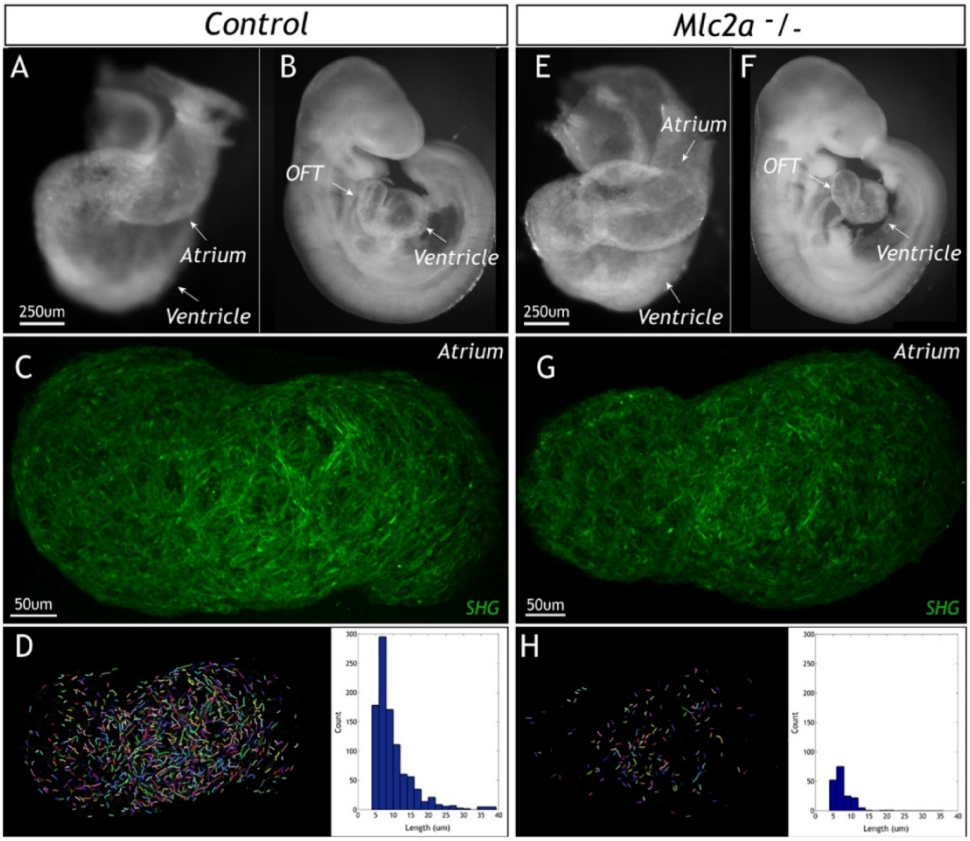

Fig. 4. SHG microscopy in a heart of a mouse mutant with reduced contractility. (A-D) Images of the control embryo. (E-H) Images of the Mlc2a KO embryo at the same developmental stage. (A and E) Brightfield microscopic image of the extracted heats and (B and F) of the whole control and Mlc2a KO embryos, respectively. (C and G) Corresponding 3-D SHG microscopy of the atria in the same control and Mlc2a KO embryos, respectively. Visualization 3 shows details of the fibrillar network 3-D organization within the atria. (D and H) quantitative visualization of SHF positive fibrillar networks in the control and Mlc2a KO embryos, respectively. The histograms show corresponding count distributions of segmented fiber lengths at the same scale. The image acquisition, rendering, visualization, and analysis for the control and the mutant embryos were performed at the same settings.

3.5 Simultaneous imaging of SHG and two-photon fluorescence of EGFP

Vital fluorescent proteins provide a valuable tool in biomedical research, as they allow for dynamic high-resolution visualization and tracking of cellular and subcellular processes without application of exogenous agents *in vivo*. A large variety of mouse lines carrying vital fluorescent reporters have been developed to investigate mammalian cardiovascular development and other physiological processes [42–45]. By spectral separation, SHG signal can be distinguished from two-photon excitation fluorescence of vital fluorescent reporters, providing an opportunity for simultaneous imaging. Generally, the level of expression of vital fluorescent reporters can be pretty high, while the SHG signal in the embryonic hearts is rather weak since the fibrillar structures are not well developed at these stages. Therefore, we then wanted to determine whether the SHG signal in early embryonic hearts is strong enough for simultaneous SHG and two-photon excitation imaging of EGFP, the most commonly used fluorescent protein. Figure 5 and Visualization 4 show simultaneous imaging of fibrillar cardiac network (green) and EGFP-labeled nuclei (red) within the cardiac wall at E9.5. The same laser wavelength of 830 nm was used as the fundamental for SHG imaging and as an

Biomedical Optics EXPRESS

excitation wavelength for two-photon microscopy. While the EGFP fluorescence signal was very strong, the details of the SHG positive fibrillar structure are well resolved without noticeable bleed-through of the EGFP signal into the SHG channel. This demonstrates that SHG and two-photon microscopy of vital fluorescent proteins can be combined for cardiac embryonic imaging.

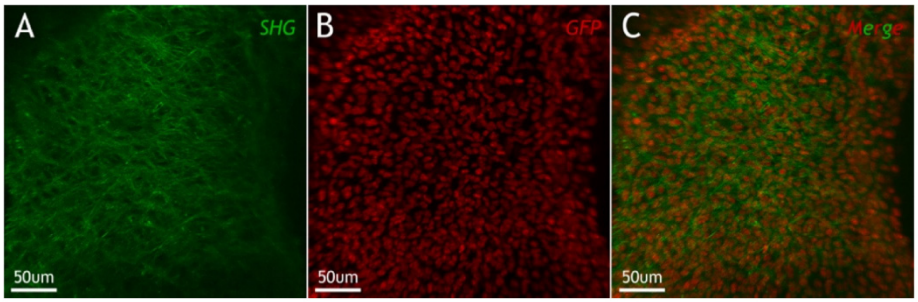

Fig. 5. Simultaneous detection of SHG and two-photon excitation imaging of EGFP in the embryonic heart. 3-D reconstruction of the cardiac wall at E9.5 (A) SHG microscopy, (B) two-photon excitation microscopy of EGFP, and (C) merged images. The volumetric view of the same area is presented in Visualization 4.

While SHG microscopy in this work was done on fixed samples for consistency and validation purposes, potentially it could be optimized for imaging of live samples. Mouse embryos can be cultured on the imaging stage at E7.5-E10.0 stages and maintained live in static culture for up to 24 hours, which allows for the investigation of developmental progression during the same embryonic stages [22,23,46]. Since SHG microscopy is a point scanning technique, direct acquisition of volumetric SHG data sets from the heart is not possible while the heart is beating. Cardiac contractions could potentially be stopped in live embryos for short intervals of time to allow for SHG acquisition. This could be done, for example, by the administration of Blebbistatin, which is commonly used to investigate conduction dynamics through optical mapping [47]. Alternatively, by taking advantage of the periodicity of the cardiac movement, one might be able to optimize gated acquisition of the SHG signal at the same phase of the cycle without stopping the contractions. Multiple retrospective and prospective gating algorithms have been developed for volumetric imaging of the beating embryonic zebrafish and mouse hearts with fluorescence microscopy and optical coherence tomography [48–50] and could potentially be implemented for SHG imaging in the beating heart.

SHG microscopy allows for imaging through the entire depth of the heart wall at early stages (until about E10.5). At later stages, as the heart grows, the imaging depth of SHG microscopy becomes a limitation. Potentially, imaging depth could be increased by application of clearing agents. Among others, a group of Prof. Valery Tuchin has made significant progress in development and application of tissue clearing compounds [51–57], which have been shown to increase imaging depth for different optical imaging methods and biological applications. Applicability of these agents for SHG imaging in mouse embryonic hearts is to be tested in future studies.

4. Summary

This paper presented SHG microscopy of fibrillar structures in mouse embryonic hearts. We demonstrated that the fibers are detectable from the earliest stages of heart contraction, and their content and organization increase significantly through the first 24 hours of heart development. SHG microscopy can clearly differentiate between fibrillar structures in different cardiac regions by as early as 10 somite stage (about 10 hours after initiation of contraction) with higher level of organization in regions of higher mechanical load. We

Biomedical Optics EXPRESS

implemented SHG microscopy in mouse model with a cardiac contractility defect, revealing reduced fibrillar content and organization. Simultaneous volumetric SHG and two-photon excitation microscopy of EGFP was demonstrated. In summary, these data suggest that SHG microscopy might be a valuable tool in investigation of biomechanical regulation of cardiac development in genetic mouse models.

Funding

National Institutes of Health (R01HL120140, R01HD096335, and T32HL07676); American Heart Association Predoctoral Fellowship (19PRE34380240).

Acknowledgments

We would like to acknowledge technical support from the Optical Imaging and Vital Microscopy (OIVM) Core at the Baylor College of Medicine.

Disclosures

The authors declare that there are no conflicts of interest related to this article.

References

1. E. J. Benjamin, P. Muntner, A. Alonso, M. S. Bittencourt, C. W. Callaway, A. P. Carson, A. M. Chamberlain, A. R. Chang, S. Cheng, S. R. Das, F. N. Delling, L. Djousse, M. S. V. Elkind, J. F. Ferguson, M. Fornage, L. C. Jordan, S. S. Khan, B. M. Kissela, K. L. Knutson, T. W. Kwan, D. T. Lackland, T. T. Lewis, J. H. Lichtman, C. T. Longenecker, M. S. Loop, P. L. Lutsey, S. S. Martin, K. Matsushita, A. E. Moran, M. E. Mussolino, M. O'Flaherty, A. Pandey, A. M. Perak, W. D. Rosamond, G. A. Roth, U. K. A. Sampson, G. M. Satou, E. B. Schroeder, S. H. Shah, N. L. Spartano, A. Stokes, D. L. Tirschwell, C. W. Tsao, M. P. Turakhia, L. B. VanWagner, J. T. Wilkins, S. S. Wong, and S. S. Virani; American Heart Association Council on Epidemiology and Prevention Statistics Committee and Stroke Statistics Subcommittee, "Heart Disease and Stroke Statistics-2019 Update: A Report From the American Heart Association," Circulation **139**(10), 56–528 (2019).
2. B. J. Martinsen and J. L. Lohr, "Handbook of Cardiac Anatomy, Physiology, and Devices," 15–23–23 (2005).
3. S. V. Biechler, L. Junor, A. N. Evans, J. F. Eberth, R. L. Price, J. D. Potts, M. J. Yost, and R. L. Goodwin, "The impact of flow-induced forces on the morphogenesis of the outflow tract," Front. Physiol. **5**, 225 (2014).
4. M. Midgett, C. S. López, L. David, A. Maloyan, and S. Rugonyi, "Increased Hemodynamic Load in Early Embryonic Stages Alters Myofibril and Mitochondrial Organization in the Myocardium," Front. Physiol. **8**, 631 (2017).
5. W. J. Kowalski, K. Pekkan, J. P. Tinney, and B. B. Keller, "Investigating developmental cardiovascular biomechanics and the origins of congenital heart defects," Front. Physiol. **5**, 408 (2014).
6. S. E. Lindsey, J. T. Butcher, and H. C. Yalcin, "Mechanical regulation of cardiac development," Front. Physiol. **5**, 318 (2014).
7. T. Mammoto and D. E. Ingber, "Mechanical control of tissue and organ development," Development **137**(9), 1407–1420 (2010).
8. D. E. Ingber, "Mechanical signaling and the Cellular Response to Extracellular Matrix in Angiogenesis and Cardiovascular Physiology," Circ. Res. **91**(10), 877–887 (2002).
9. M. Rienks, A.-P. Papageorgiou, N. G. Frangogiannis, and S. Heymans, "Myocardial Extracellular Matrix," Circ. Res. **114**(5), 872–888 (2014).
10. K. Imanaka-Yoshida and H. Aoki, "Tenascin-C and mechanotransduction in the development and diseases of cardiovascular system," Front. Physiol. **5**, 283 (2014).
11. L. K. Hornberger, S. Singhroy, T. Cavalle-Garrido, W. Tsang, F. Keeley, and M. Rabinovitch, "Synthesis of Extracellular Matrix and Adhesion Through β(1) Integrins are Critical for Fetal Ventricular Myocyte Proliferation," Circ. Res. **87**(6), 508–515 (2000).
12. W. Carver, M. L. Nagpal, M. Nachtigal, T. K. Borg, and L. Terracio, "Collagen expression in mechanically stimulated cardiac fibroblasts," Circ. Res. **69**(1), 116–122 (1991).
13. E. Nam, W. C. Lee, and S. Takeuchi, "Formation of Highly Aligned Collagen Nanofibers by Continuous Cyclic Stretch of a Collagen Hydrogel Sheet," Macromol. Biosci. **16**(7), 995–1000 (2016).
14. A. S. Piotrowski-Daspit, B. A. Nerger, A. E. Wolf, S. Sundaresan, and C. M. Nelson, "Dynamics of Tissue-Induced Alignment of Fibrous Extracellular Matrix," Biophys. J. **113**(3), 702–713 (2017).
15. N. K. Weidenhamer and R. T. Tranquillo, "Influence of cyclic mechanical stretch and tissue constraints on cellular and collagen alignment in fibroblast-derived cell sheets," Tissue Eng. Part C Methods **19**(5), 386–395 (2013).
16. J. Liu, W. Yu, Y. Liu, S. Chen, Y. Huang, X. Li, C. Liu, Y. Zhang, Z. Li, J. Du, C. Tang, J. Du, and H. Jin, "Mechanical stretching stimulates collagen synthesis via down-regulating SO2/AAT1 pathway," Sci. Rep. **6**(1), 21112 (2016).

Biomedical Optics EXPRESS

17. V. Gupta and K. J. Grande-Allen, "Effects of static and cyclic loading in regulating extracellular matrix synthesis by cardiovascular cells," Cardiovasc. Res. **72**(3), 375–383 (2006).
18. G. Cox, E. Kable, A. Jones, I. Fraser, F. Manconi, and M. D. Gorrell, "3-Dimensional imaging of collagen using second harmonic generation," J. Struct. Biol. **141**(1), 53–62 (2003).
19. L. Mostaço-Guidolin, N. L. Rosin, and T.-L. Hackett, "Imaging Collagen in Scar Tissue: Developments in Second Harmonic Generation Microscopy for Biomedical Applications," Int. J. Mol. Sci. **18**(8), 1772 (2017).
20. N. H. Green, R. M. Delaine-Smith, H. J. Askew, R. Byers, G. C. Reilly, and S. J. Matcher, "A new mode of contrast in biological second harmonic generation microscopy," Sci. Rep. **7**(1), 13331 (2017).
21. S. V. Plotnikov, A. C. Millard, P. J. Campagnola, and W. A. Mohler, "Characterization of the Myosin-Based Source for Second-Harmonic Generation from Muscle Sarcomeres," Biophys. J. **90**(2), 693–703 (2006).
22. A. L. Lopez 3rd, S. Wang, K. V. Larin, P. A. Overbeek, and I. V. Larina, "Live four-dimensional optical coherence tomography reveals embryonic cardiac phenotype in mouse mutant," J. Biomed. Opt. **20**(9), 090501 (2015).
23. A. L. Lopez, M. D. Garcia, M. E. Dickinson, and I. V. Larina, "Live Confocal Microscopy of the Developing Mouse Embryonic Yolk Sac Vasculature," in *Vascular Morphogenesis: Methods and Protocols*, D. Ribatti, ed. (Springer New York, New York, NY, 2015), pp. 163–172.
24. J. R. Prigge, J. A. Wiley, E. A. Talago, E. M. Young, L. L. Johns, J. A. Kundert, K. M. Sonsteng, W. P. Halford, M. R. Capecchi, and E. E. Schmidt, "Nuclear double-fluorescent reporter for in vivo and ex vivo analyses of biological transitions in mouse nuclei," Mamm. Genome **24**, 389–399 (2013).
25. E. G. Stanley, C. Biben, A. Elefanty, L. Barnett, F. Koentgen, L. Robb, and R. P. Harvey, "Efficient Cre-mediated deletion in cardiac progenitor cells conferred by a 3'UTR-ires-Cre allele of the homeobox gene Nkx2-5," Int. J. Dev. Biol. **46**, 431–443 (2004).
26. C. Huang, F. Sheikh, M. Hollander, C. Cai, D. Becker, P.-H. Chu, S. Evans, and J. Chen, "Embryonic atrial function is essential for mouse embryogenesis, cardiac morphogenesis and angiogenesis," Development **130**(24), 6111–6119 (2003).
27. W. Supatto, D. T. T. F. Debarre, E. D. D F. Beaurepaire, and E. Beaurepaire, "Advances in multiphoton microscopy for imaging embryos," Curr. Opin. Genet. Dev. **21**(5) 538–548 (2011).
28. N. Olivier, K. Aptel, F. F. Plamann, M. C. Plamann, K. F. S. Klein, E. S. K. M. F. Beaurepaire, and E. Beaurepaire, "Harmonic microscopy of isotropic and anisotropic microstructure of the human cornea," Opt. Express **18**(5), 5028–5040 (2010).
29. M. Rehberg, U. Krombach, F. F. Pohl, S. Pohl, U. F. Dietzel, and S. Dietzel, "Label-free 3D visualization of cellular and tissue structures in intact muscle with second and third harmonic generation microscopy," PLoS ONE **6**(11), e28237 (2011).
30. S. Dietzel, J. Pircher, A. K. Nekolla, M. Gull, A. W. Brandli, U. Pohl, and M. Rehberg, "Label-free determination of hemodynamic parameters in the microcirculaton with third harmonic generation microscopy," PLoS ONE **9**(6), e99615 (2014).
31. C. Misra and V. Garg, "Compacting the heart with Notch," Nat. Med. **19**(2), 133–134 (2013).
32. M. Midgett and S. Rugonyi, "Congenital heart malformations induced by hemodynamic altering surgical interventions," Front. Physiol. **5**, 287 (2014).
33. M. W. Jenkins, O. Q. Chughtai, A. N. Basavanhally, M. Watanabe, and A. M. Rollins, "In vivo gated 4D imaging of the embryonic heart using optical coherence tomography," J. Biomed. Opt. **12**(3), 030505 (2007).
34. M. W. Jenkins, A. R. Duke, S. Gu, H. J. Chiel, H. Fujioka, M. Watanabe, E. D. Jansen, and A. M. Rollins, "Optical pacing of the embryonic heart," Nat. Photonics **4**(9), 623–626 (2010).
35. I. V. Larina, N. Sudheendran, M. Ghosn, J. Jiang, A. Cable, K. V. Larin, and M. E. Dickinson, "Live imaging of blood flow in mammalian embryos using Doppler swept-source optical coherence tomography," J. Biomed. Opt. **13**(6), 060506 (2008).
36. I. V. Larina, K. Furushima, M. E. Dickinson, R. R. Behringer, and K. V. Larin, "Live imaging of rat embryos with Doppler swept-source optical coherence tomography," J. Biomed. Opt. **14**(5), 050506 (2009).
37. N. Sudheendran, S. H. Syed, M. E. Dickinson, I. V. Larina, and K. V. Larin, "Speckle variance OCT imaging of the vasculature in live mammalian embryos," Laser Phys. Lett. **8**(3), 247–252 (2011).
38. S. H. Syed, K. V. Larin, M. E. Dickinson, and I. V. Larina, "Optical coherence tomography for high-resolution imaging of mouse development in utero," J. Biomed. Opt. **16**(4), 046004 (2011).
39. S. Bhat, I. V. Larina, K. V. Larin, M. E. Dickinson, and M. Liebling, "4D reconstruction of the beating embryonic heart from two orthogonal sets of parallel optical coherence tomography slice-sequences," IEEE Trans. Med. Imaging **32**(3), 578–588 (2013).
40. M. D. Garcia, A. L. Lopez 3rd, K. V. Larin, and I. V. Larina, "Imaging of cardiovascular development in Mammalian embryos using optical coherence tomography," Methods Mol. Biol. **1214**, 151–161 (2015).
41. P. M. Kulkarni, N. Rey-Villamizar, A. Merouane, N. Sudheendran, S. Wang, M. Garcia, I. V. Larina, B. Roysam, and K. V. Larin, "Algorithms for improved 3-D reconstruction of live mammalian embryo vasculature from optical coherence tomography data," Quant. Imaging Med. Surg. **5**(1), 125–135 (2015).
42. J. J. Armstrong, I. V. Larina, M. E. Dickinson, W. E. Zimmer, and K. K. Hirschi, "Characterization of bacterial artificial chromosome transgenic mice expressing mCherry fluorescent protein substituted for the murine smooth muscle alpha-actin gene," Genesis **48**(7), 457–463 (2010).

Biomedical Optics EXPRESS

43. I. V. Larina, W. Shen, O. G. Kelly, A.-K. Hadjantonakis, M. H. Baron, and M. E. Dickinson, "A Membrane Associated mCherry Fluorescent Reporter line for Studying Vascular Remodeling and Cardiac Function During Murine Embryonic Development," Anat. Rec. (Hoboken) **292**(3), 333–341 (2009).
44. M. A. Dyer, D. F. S. F. Mohn, J. R. Mohn, D F. Munday, M. H. M. J F. Baron, and M. H. Baron, "Indian hedgehog activates hematopoiesis and vasculogenesis and can respecify prospective neurectodermal cell fate in the mouse embryo."
45. A. Acharya, S. T. Baek, G. Huang, B. Eskiocak, S. Goetsch, C. Y. Sung, S. Banfi, M. F. Sauer, G. S. Olsen, J. S. Duffield, E. N. Olson, and M. D. Tallquist, "The bHLH transcription factor Tcf21 is required for lineage-specific EMT of cardiac fibroblast progenitors," Development **139**(12), 2139–2149 (2012).
46. E. A. Jones, D. Crotty, P. M. Kulesa, C. W. Waters, M. H. Baron, S. E. Fraser, and M. E. Dickinson, "Dynamic in vivo imaging of postimplantation mammalian embryos using whole embryo culture," Genesis **34**(4), 228–235 (2002).
47. M. C. Rémond, J. A. Fee, E. L. Elson, and L. A. Taber, "Myosin-based contraction is not necessary for cardiac c-looping in the chick embryo," Anat. Embryol. (Berl.) **211**(5), 443–454 (2006).
48. M. Liebling, A. S. Forouhar, M. Gharib, S. E. Fraser, and M. E. Dickinson, "Four-dimensional cardiac imaging in living embryos via postacquisition synchronization of nongated slice sequences," J. Biomed. Opt. **10**(5), 054001 (2005).
49. S. Bhat, I. V. Larina, K. V. Larin, M. E. Dickinson, and M. Liebling, "Multiple-cardiac-cycle noise reduction in dynamic optical coherence tomography of the embryonic heart and vasculature," Opt. Lett. **34**(23), 3704–3706 (2009).
50. J. M. Taylor, J. M. Girkin, and G. D. Love, "High-resolution 3D optical microscopy inside the beating zebrafish heart using prospective optical gating," Biomed. Opt. Express **3**(12), 3043–3053 (2012).
51. V. V. Tuchin, *Optical Clearing of Tissues and Blood* (SPIE, Bellingham, 2005).
52. D. Zhu, K. V. Larin, Q. Luo, and V. V. Tuchin, "Recent progress in tissue optical clearing," Laser Photonics Rev. **7**(5), 732–757 (2013).
53. A. Sdobnov, M. E. Darvin, J. Lademann, and V. Tuchin, "A comparative study of ex vivo skin optical clearing using two-photon microscopy," J. Biophotonics **10**(9), 1115–1123 (2017).
54. S. Masoumi, M. A. Ansari, E. Mohajerani, E. A. Genina, and V. V. Tuchin, "Combination of analytical and experimental optical clearing of rodent specimen for detecting beta-carotene: phantom study," J. Biomed. Opt. **23**(9), 1–7 (2018).
55. L. M. Oliveira, M. I. Carvalho, E. M. Nogueira, and V. V. Tuchin, "Skeletal muscle dispersion (400-1000 nm) and kinetics at optical clearing," J. Biophotonics **11**(1), e201700094 (2018).
56. A. Y. Sdobnov, M. E. Darvin, J. Schleusener, J. Lademann, and V. V. Tuchin, "Hydrogen bound water profiles in the skin influenced by optical clearing molecular agents-Quantitative analysis using confocal Raman microscopy," J. Biophotonics, 201800283 (2018).
57. I. V. Larina, E. F. Carbajal, V. V. Tuchin, M. E. Dickinson, and K. V. Larin, "Enhanced OCT imaging of embryonic tissue with optical clearing," Laser Phys. Lett. **5**(6), 476–479 (2008).